https://dx.doi.org/10.1016/j.precisioneng.2021.09.010

Maskless fluid jet polishing of optical structured surfaces

Chunjin Wang[1], Zili Zhang[1], Chi Fai Cheung[1]*, Wang Luo[2], Yee Man Loh[1], Yanjun Lu[2]*, Lingbao Kong[3], Shixiang Wang[3]

[1] *State Key Laboratory of Ultra-precision Machining Technology, Department of Industrial and Systems Engineering, The Hong Kong Polytechnic University, Hung Hom, Kowloon, Hong Kong, China*

[2] *Guangdong Provincial Key Laboratory of Micro/Nano Optomechatronics Engineering, College of Mechatronics and Control Engineering, Shenzhen University, Shenzhen, 518060, China*

[3] *Shanghai Engineering Research Center of Ultra-Precision Optical Manufacturing, Fudan University, Shanghai, PR China*

* Corresponding author: benny.cheung@polyu.edu.hk, luyanjun@szu.edu.cn.

Abstract

Various kinds of optical structured surface have been widely used in different fields, such as imaging and illumination. However, the machining process of the optical structured surface usually leaves tool marks, burs, debris and defects on the structured surface. Currently, it is still a challenging problem to remove these kinds of defects and further improve the surface quality effectively, to obtain better functional performance. In this paper, maskless fluid jet polishing (MFJP) is innovatively presented which is an attempt to solve this problem. In MFJP, low pressure micro abrasive water jet slurry is impinged on the structured surface to implement tiny material removal without using a mask. Experimental investigations on the polishing of sinusoidal structured surface and V-groove structured surface were performed to realize the technical feasibility of MFJP on structured surface, based on the analysis of surface roughness, form maintainability, and surface smoothness. A computational fluid dynamics (CFD) model was also developed to simulate the MFJP process on V-groove surface to demonstrate the fluid flow movement and material removal characteristics. In addition, the effect of the key

polishing parameters was also studied and discussed. The results indicate that MFJP can significantly improve the surface quality of optical structured surface, while possessing high form maintainability under certain conditions. It may become a competitive method for the precision polishing of optical structured surfaces. And this study also sheds some light on the application of MFJP for the polishing of other kinds of surfaces with small or micrometer scale cavities or channels, such as microfluidic chips, etc.

Keywords

Fluid jet polishing, optical structured surface, finishing, abrasive water jet, ultra-precision machining, computational fluid dynamics, maskless

1. Introduction

Structured surface possesses a regular and periodic pattern and can realize specific functions such as optical, physical, and biological [1]. In recent years, due to the rapid development of industries such as optical fiber communication and imaging technology, tiny components with structured optical functional surfaces of a small size, light weight, and high integration, are widely used in optoelectronics and communication products, biomedical, automotive lighting, and other fields [2]. Typical optical structured surfaces are optical micro lens arrays, Fresnel lens structures, artificial optical compound eyes, V-shaped or cylindrical groove structured arrays, reflective prism arrays, etc. [3, 4]. Driven by a large demand and expensive processing costs for single components, high-precision injection molding has been widely used for the mass production [5] of structured surface components. To improve the replication stability and extend the mold life, difficult-to-machine material such as stainless steel, tungsten carbide, or silicon carbide, are used as the mold material.

Various methods have been developed for the generation of structured surfaces, including milling [6], turning [7], grinding [8], chiseling [9], electrical discharge machining [10], laser machining [11], abrasive jet machining [12], etc. However, these machining methods often leave tool marks, burs, debris and defects on the surface. In

most cases, the surface quality after direct machining cannot meet the practical and functional requirements, and subsequent polishing is required.

To meet the increasing demand for high-accuracy optical structured surfaces, several different kinds of polishing methods have been developed to improve the surface quality of the structured surface, such as copying tool polishing, magnetic field-assisted polishing, vibration or vibration-assisted polishing, etc. The polishing of optical structured surface aims to improve the surface roughness without degrading the form accuracy of the featured structure. Brinksmeier et al. [13] presented the pen-shaped and wheel-shaped copying tools to polish a structured array on mold steel (X40Cr13) and electroless nickel-plated steel. The surface roughness after polishing reached 4.5 nm. Other researchers also successfully used the copying tool for the polishing of structures such as v-groove array [14-15], cylindrical structure array [16-17], Fresnel surface [18], etc.

However, the copying tool polishing method has some limitations, such as tool wear, specific design of tool for different kinds of structures, and high requirement regarding the motion accuracy of the polishing machine. Different kinds of magnetic field-assisted finishing methods have also been developed for the polishing of structured surface, such as magnetic abrasive polishing [19-21], magnetorheological fluid polishing [22-25], and magnetic compound finishing [26-28]. Nanometer or sub-nanometer scale surface roughness of the structured surface can be successfully achieved by the magnetic field-assisted polishing method. Nevertheless, there is still a big challenge to maintain the form of the featured structure, especially for surface structures with a high aspect ratio. Moreover, there also exists a material limitation problem when adopting the magnetic field-assisted polishing method. Different kinds of vibration or vibration-assisted polishing have also been proposed for the polishing of structured surfaces [29-34], while these methods still have the limitations as mentioned of the copying tool polishing method. Matsumura et al. [35] attempted the abrasive water jet polishing of the V-groove adopting relatively high pressure (15~35 MPa) with the help of mask. Moreover, the shape of the mask was purposely designed to obtain a larger stagnation zone to increase the size of the crack-free zone during

polishing. The surface roughness of the groove was successfully improved from 46 nm to 25 nm in Ra. Nonetheless, it is difficult to make a purposely designed mask for structured array surface, which also largely increases the polishing cost. Moreover, high-pressure abrasive water jets can easily generate brittle fracture, leading to poor surface roughness.

On the whole, most of the existing structured polishing methods have certain technical limitations, such as structure form maintainability, material limitation, and shape limitation. In addition, traditional mechanical polishing methods can hardly adapt to the structured surface form. Hence, a mature and generic polishing method is still greatly needed to meet the increasing demand for ultra-precision optical structured surfaces. In this paper, an innovative maskless fluid jet polishing (MFJP) method is presented which attempts to solve the problems mentioned above. In MFJP, a low-pressure (normally less than 15 bar) micro abrasive water jet slurry is impinged on the structured surface to implement tiny material removal without using a mask. The working principle of the process is presented in section 2. Section 3 presents the design of the experiments so as to investigate the polishing performance on sinusoidal structured surface and V-groove structured surface. Section 4 presents the experimental results, as well as the discussion based on the computational fluidic dynamics (CFD) simulation model built for the MFJP process. Finally, a conclusion is presented to summarize the research work in this paper in section 5.

2. Maskless fluid jet polishing methods

An abrasive water jet polishing method under relatively low pressure (also called 'fluid jet polishing (FJP)'), proposed by Fähnle et al. [36], has been widely used in the polishing of optical lenses and molds, including spherical/aspherical or freeform surfaces. During FJP, abrasive at the micro/nano meter scale is evenly mixed with water pumped out of a nozzle, and impinges the target surface to implement material removal through an erosion process. The fluid jet is highly flexible, which can easily adapt to surface with complicated geometry. It can be used for the polishing of most kinds of materials, including ceramic, metal, glass, etc. Hence, why not try polishing optical

structured surface using FJP? Considering that a mask is needed under a high-pressure abrasive water jet, a mask may not be necessary for low-pressure FJP which can not only greatly reduce the polishing cost, but also make the polishing process much easier.

Hence, a series of experimental and theoretical investigations of the polishing performance of maskless fluid jet polishing (MFJP) on optical structured surface were conducted in this study. Fluid pressure of less than 15 bar is normally adopted in MFJP, and no mask is used. Fig. 1 shows a schematic diagram of MFJP on structured surface. In this study, the structured surfaces were divided into continuous structured surface and discontinuous structured surface. The continuous structure here refers to a structure with no sharp edge (e.g., wavy structure, sinusoidal structure, etc.), and others are the discontinuous structured surface (e.g., V-groove structure array, lenticular lens array, etc.) as shown in Fig. 1.

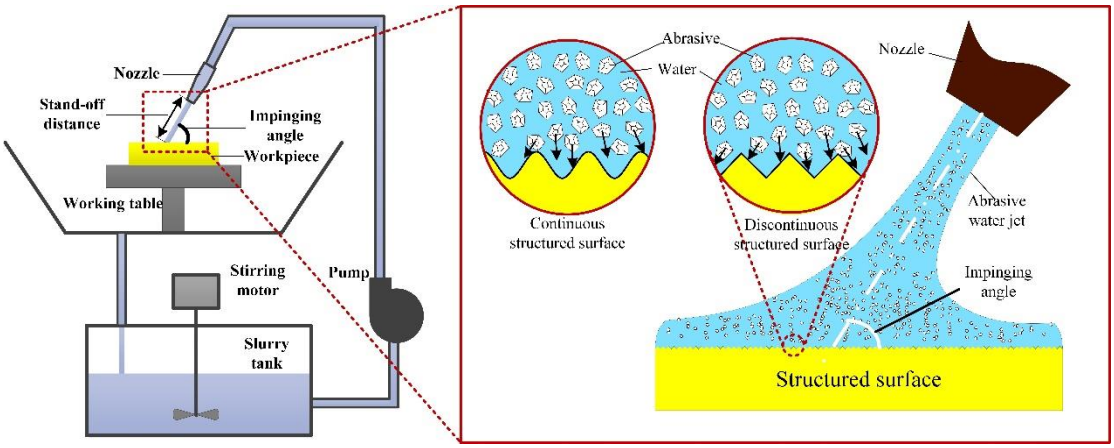

Fig. 1 Schematic diagram of the maskless fluid jet polishing (MFJP) of structured surface

3. Experimental procedures

The experiments were conducted on a *ZEEKO IRP200* polishing machine as shown in Fig. 2. Two kinds of structured surfaces were tested in this study to represent the polishing performance on both continuous structured surface and discontinuous structured surface, respectively. One of the workpieces was a sinusoidal structured surface made of S136 mold steel, which is the mold of the flood lighting component, implementing the function of transforming a surface source to a line source. The

sinusoidal structured surface was machined by electrical discharge machining (EDM), with surface arithmetic roughness (Ra) of between 400 and 700 nm. The other one was V-groove structured surface made of S136H mold steel as shown in the right bottom part of Fig. 2. It is the mold for a LED diffusion plate, which is machined by a V-tip grinding wheel with surface roughness ranging from 90 nm-170 nm, as reported by Lu et al. [37]. One sapphire nozzle with a diameter of 0.5 mm was used, and the polishing slurry was silicon carbide abrasive (average particle size of 11.9 μm, GC 1000#, FUJIMI, Corp.) mixed with pure water with the weight percentage of 10%. Table 1 summarizes the polishing conditions on the sinusoidal structured surface. The whole surface was polished thoroughly by three passes of polishing to demonstrate its polishing performance. The polishing experiment on the V-groove surface was divided into four groups to investigate the polishing performance and the effect of some key polishing parameters, including feed rate, fluid pressure, impinging angle and stand-off distance. Table 2 summarizes the polishing conditions. The material of the V-groove mold surface was S136H with a hardness of 30-35HRC. Two regions with a size of 3 mm × 3 mm on the V-groove surface were polished under each condition.

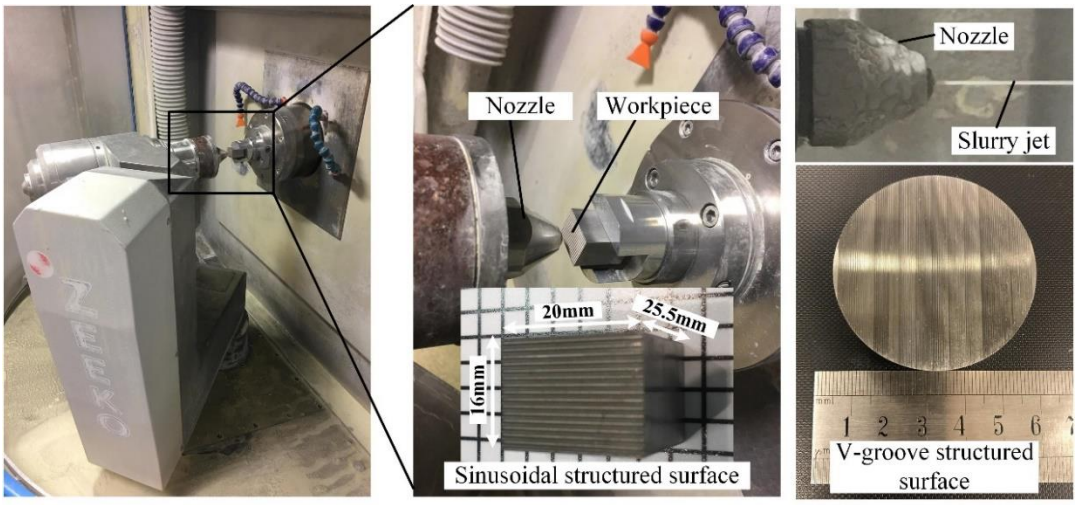

Fig. 2 Experimental setup

Table 1 Polishing conditions for the sinusoidal structured surface

Conditions	Value
Fluid pressure	10 bar
Impinging angle	90 degrees
Stand-off distance (SOD)	2 mm
Feed rate	50 mm/min
Tool path	Raster path with 0.2 mm scan interval
Polishing time	3 passes of polishing, 32.4 min for each pass

The surface topography of the sinusoidal structured surface before and after polishing was characterized by a *Hitachi* Electron Microscope *TM3000* with magnifications of 150, 1000, and 5000. The surface roughness was measured on a *Zygo Nexview* white light 3D interferometer. The magnification of the object lens was 40. The lateral and vertical resolutions of the measurement were 208.8 nm and 0.1 nm, respectively. The arithmetic average surface roughness (*Sa*) was defined according to ISO25178 standard. The surface roughness was analyzed using the software *MX*. A nine-order polynomial filter was used, and other settings were the default settings of the software. Considering the small effective area for surface roughness measurement in the bottom area of the sinusoidal surface, a region of around 50 μm×50 μm was used as the measurement area of both bottom and top surface of the sinusoidal structured surface. The 3D surface form of the sinusoidal structured surface was measured by a *Form Talysurf PGI* 1240 profilometer. A 60 mm arm with 2 μm radius conisphere diamond stylus was used. The vertical and lateral resolutions were 0.8 nm and 0.25 μm, respectively. Considering the high surface gradient of the V-groove, leading to missing data when measured on a white light interferometer, an *Alpha-Step D300* profiler (*KLA-Tencor*, California, USA) was used to measure the surface profile and surface roughness. The vertical and lateral resolutions were 0.038 nm and 100 nm, respectively. The surface roughness was determined according to ISO 4287:1997 standard.

Moreover, the surface microscale topography was characterized on a high-resolution scanning electron microscope (SEM, Quanta 450 FEG, FEI Company, Hillsboro, USA).

Table 2 Polishing conditions for the V-groove structured surface

Conditions	Group 1	Group 2	Group 3	Group 4
Feed rate (mm/min)	10,20,30,40,60,80,100	30	30	30
Fluid pressure (bar)	8	6,8,10,12	8	8
Impinging angle (˚)	90	90	45,60,75,90	90
Stand-off distance (mm)	4	4	4	2,4,6,8,10
Tool path	Raster path with 0.1 mm scan interval			
Polishing time (min)	1 pass of 9.3, 4.7, 3.1, 2.4, 1.6, 1.2, 1.0 min	1 pass of 3.1 min		

4. Results and discussion

4.1 Polishing performance on the sinusoidal structured array surface

4.1.1 Analysis of surface topography

Fig. 3 shows snapshots of the sinusoidal surface before and after polishing. The surface after polishing becomes much more shiny as compared to the initial surface. The SEM measurement results were obtained on the top, side, and bottom surfaces of the sinusoidal surface under three different magnifications. As shown in Fig. 4, typical discharge craters after EDM could be easily found on the initial surface [38]. These defects were thoroughly removed after polishing, only leaving tiny abrasive erosion marks. SEM photos on the edge were also compared as shown in Fig. 5. It was found that the surface after polishing was much smoother than the initial surface. Meanwhile, the form at the sharp edge was also maintained well.

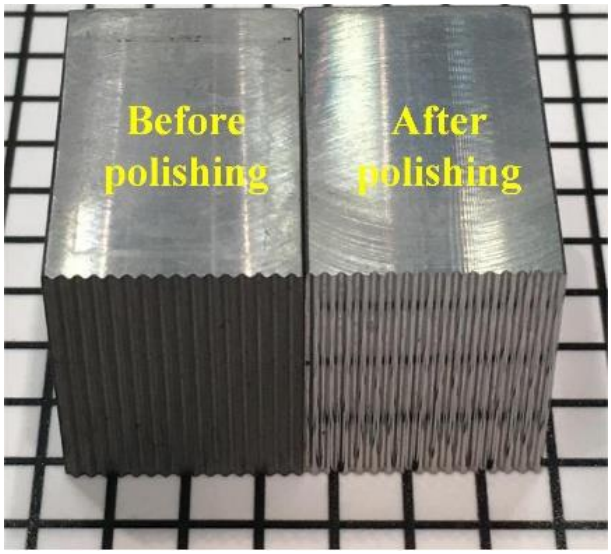

Fig. 3 Snapshots of the sinusoidal structured surface before and after polishing

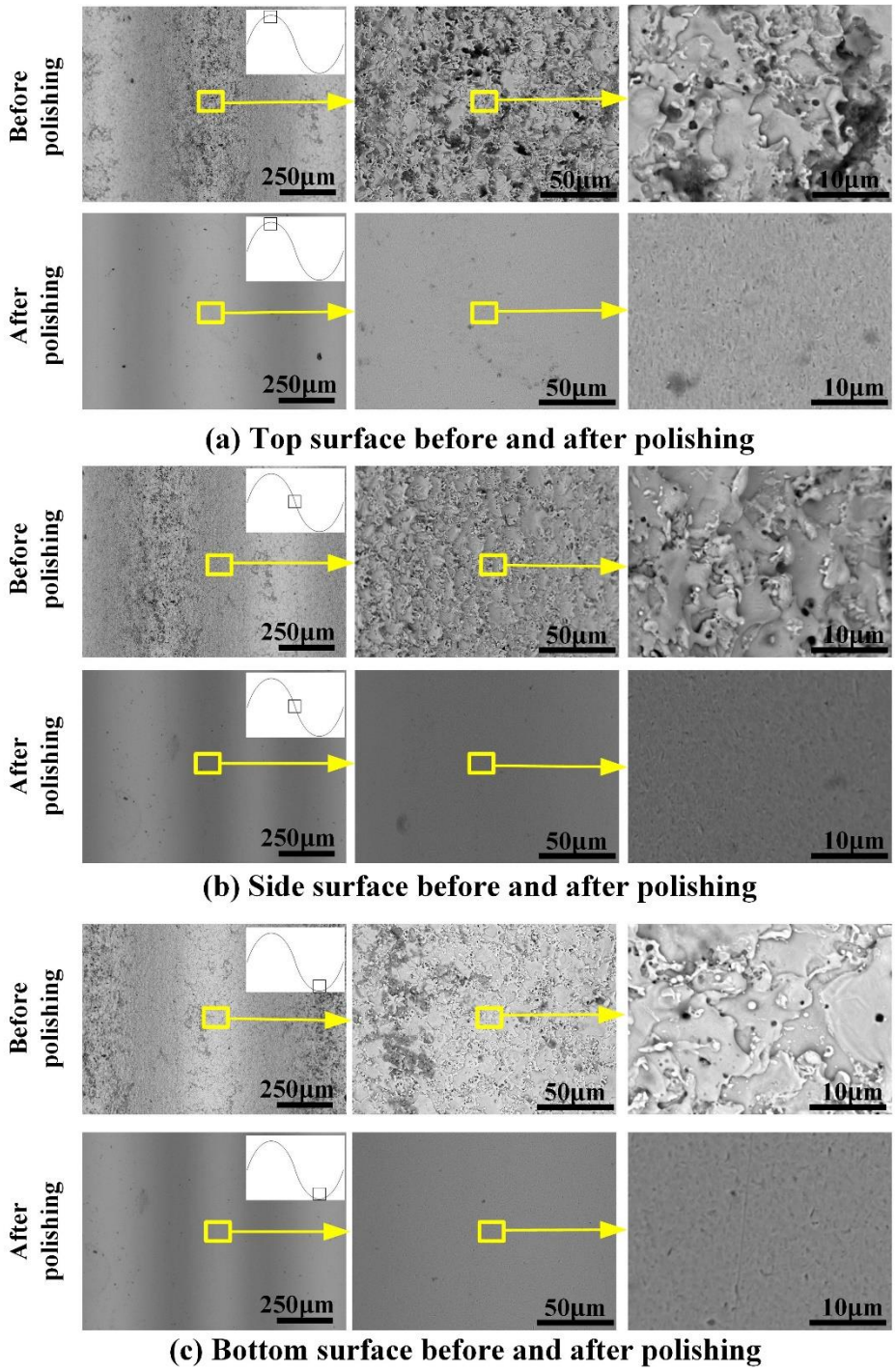

Fig. 4 SEM photos of the sinusoidal structured surface before and after polishing under three different magnifications

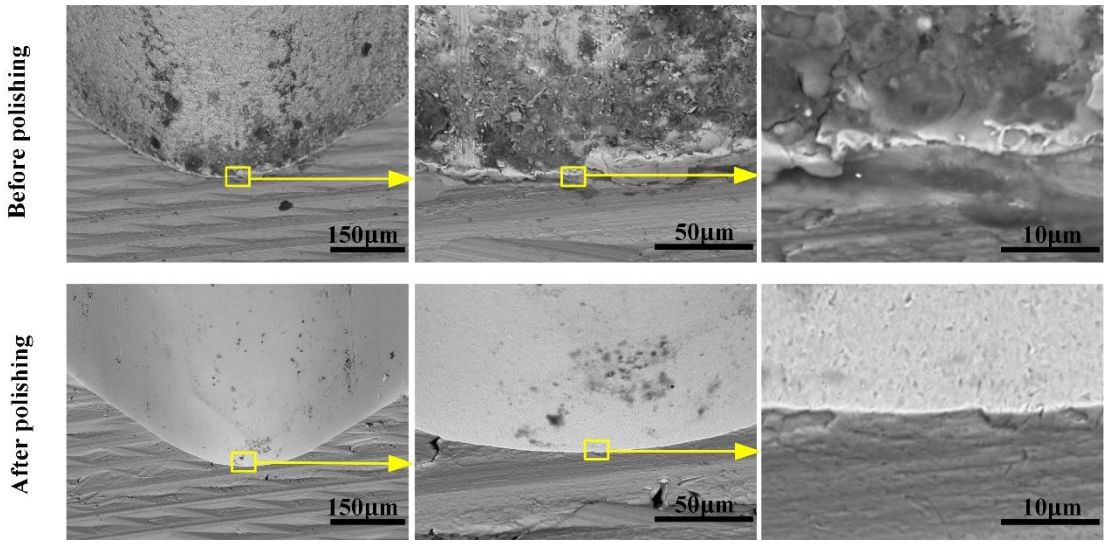

Fig. 5 SEM photos of the edge surface before and after polishing

The surface roughness measurement results are presented in Fig. 6. The Sa on the top and bottom surface before polishing were 642.1 nm and 458.9 nm, respectively. After polishing, the Sa of the top and bottom surface was reduced to 18.8 nm and 14.4 nm, respectively. The convergence ratio of the surface roughness is defined as

$$\eta_{Sa} = \frac{Sa_{initial} - Sa_{after\_polishing}}{Sa_{initial}} \times 100\% \quad (1)$$

where $Sa_{initial}$ is the Sa of the initial surface, while $Sa_{after\_polishing}$ is the Sa after polishing. The η_{Sa} reached more than 96%, which proves that MFJP is effective in reducing the surface roughness of the sinusoidal structured surface and has the potential for the polishing of other kinds of continuous structured surfaces. Furthermore, the polishing efficiency could be further enhanced by the application of multi-jet polishing [39] or fluid line jet polishing [40].

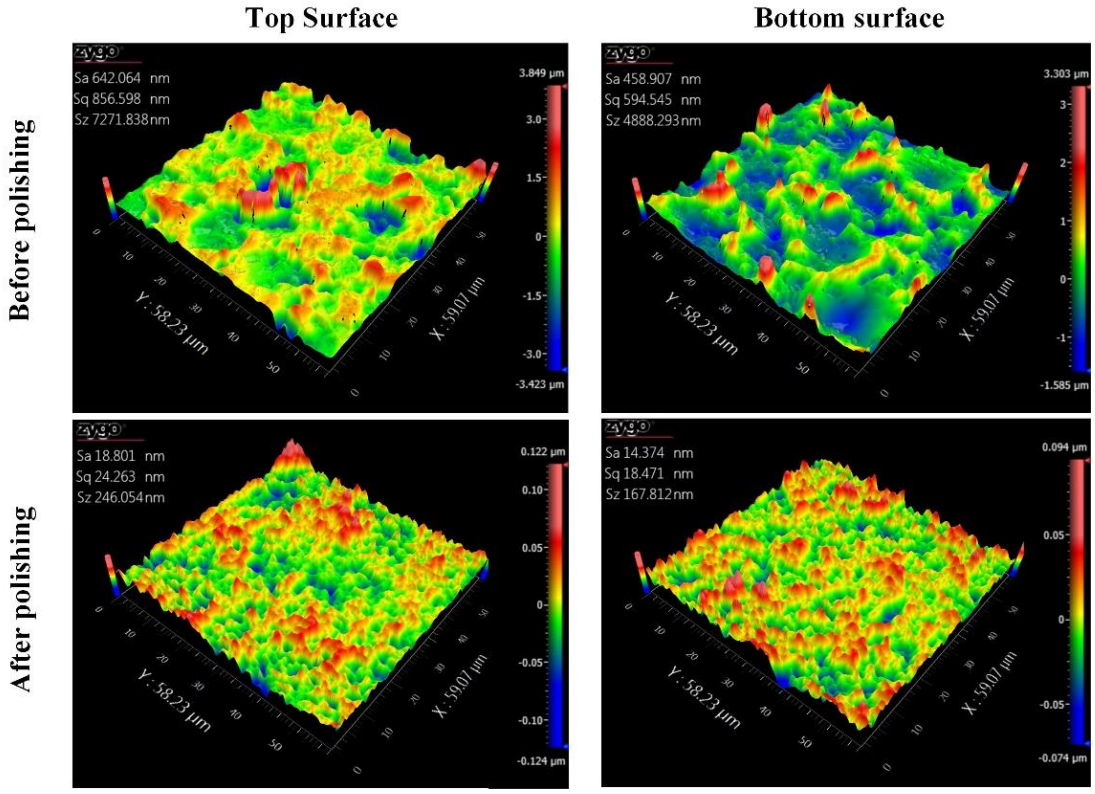

Fig. 6 Surface roughness comparison of the sinusoidal structured surface before and after polishing

4.1.2 Analysis of surface form maintainability

Except for surface topography, surface form maintainability is also an important evaluation index in structured surface polishing. A Form Talysurf PGI1240 was used to measure the surface profile before and after polishing. Fig. 7(a) and Fig. 7(b) show the measured surface profile before and after polishing, respectively. For better analysis, they were matched based on the anyDOF registration algorithm [41] and compared as shown in Fig. 7(c) and Fig. 7(d). It was found that the surface profile was maintained well as shown in the sectional profile comparison results, and the smoothening of the surface can also be clearly observed in Fig. 7(c).

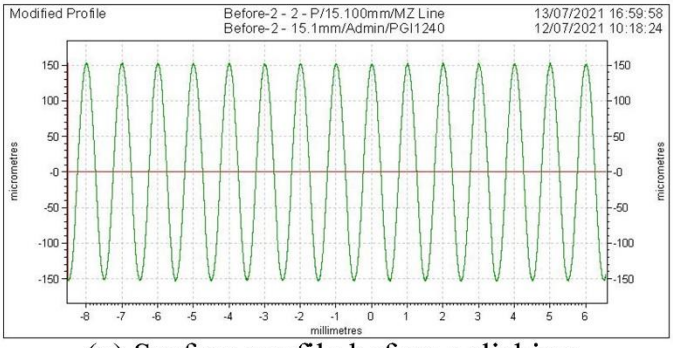

(a) Surface profile before polishing

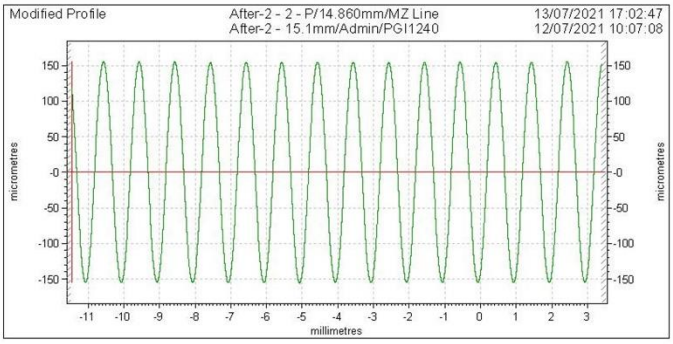

(b) Surface profile after polishing

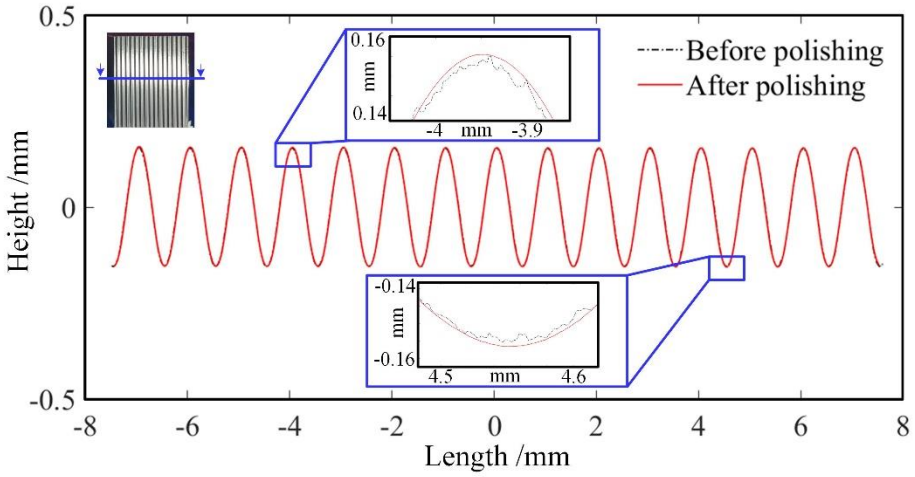

(c) Surface profile comparison

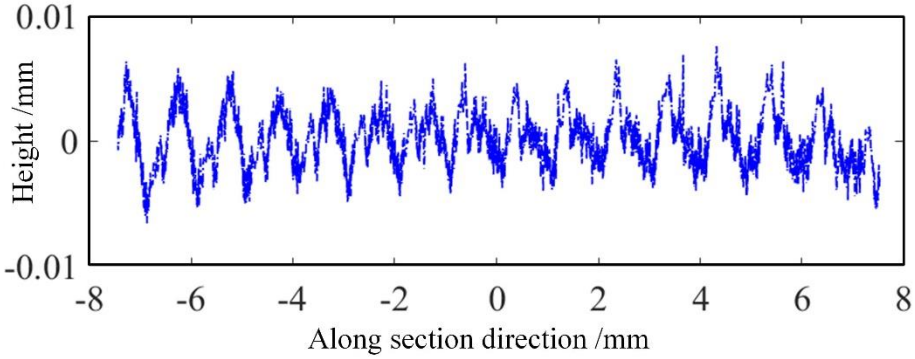

(d) Form deviation

Fig. 7 Analysis of the sinusoidal structured surface profile before and after polishing

In order to compare them quantitatively, the maintenance ratio η is defined here for better comparison, which is expressed as

$$\begin{aligned}\eta &= \left[1-\left|\frac{H_{before\_polishing}-H_{after\_polishing}}{H_{before\_polishing}}\right|\right]\times 100\% \\ &= \left[1-\left|\frac{\left(h_{peak}-h_{bottom}\right)-\left(h_{0\_peak}-h_{0\_bottom}\right)}{h_{0\_peak}-h_{0\_bottom}}\right|\right]\times 100\%\end{aligned} \tag{2}$$

where $H_{before\_polishing}$ and $H_{after\_polishing}$ are the height between the peak and bottom of the structure feature before and after polishing, respectively. h_{0_peak} and h_{0_bottom} are the height of the peak and bottom before polishing, while h_{peak} and h_{bottom} are the height of the peak and bottom after polishing. The form maintenance ratio η of the sinusoidal structured surface after MFJP reached 99.2%, which indicates high form maintainability.

4.2 Polishing performance on V-groove structured array surface

Fig. 8 shows the surface roughness of the V-groove surface after polishing under different feed rates. The surface arithmetic roughness Ra was calculated through Eq. (3) [42] based on the data measured on the *Alpha-Step D300* profiler (KLA-Tencor, California, USA), considering the limited measurement depth and surface gradient of the *Zygo Nexview* white light 3D interferometer.

$$Ra = \frac{1}{L}\int_0^L |h|\,dx \tag{3}$$

where L is the sampling length which was 50 μm in this study, h is the profile height at each position. The data were collected at three different positions of each V-groove surface under each condition. It can be seen that the surface roughness was largely reduced after one pass of the fluid jet polishing, even under the feed rate of 100 mm/min (~1 min of the polishing time). Smaller surface roughness was obtained with a slower feed rate, corresponding to longer polishing time. When the feed rate was 10 mm/min, the average surface roughness was reduced from 132.5 nm to 40.6 nm after one pass of polishing (~9.3 min of polishing time). Selected SEM photographs of the polished

surface under different feed rates are also provided in Fig. 9 to compare the surface quality after polishing. It is found that severe grinding marks on the V-groove surface were gradually removed under a slower feed rate. This is due to the fact that a slower feed rate results in longer polishing time and hence larger material removal. Moreover, the grinding marks were almost completely removed when the feed rate was less than 30 mm/min. This result indicates that MFJP is also effective in improving the surface roughness of V-groove structured surface, which is a typical type of non-continuous structured surface.

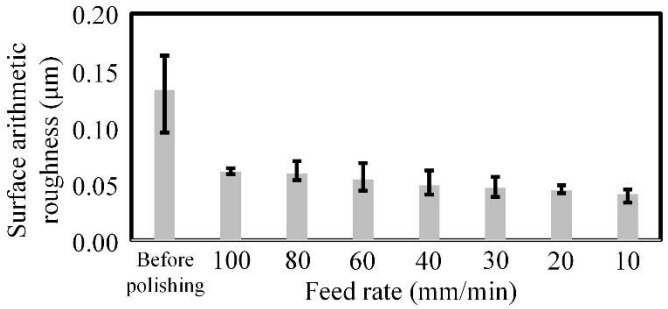

Fig. 8 Measured surface roughness varies with the feed rate

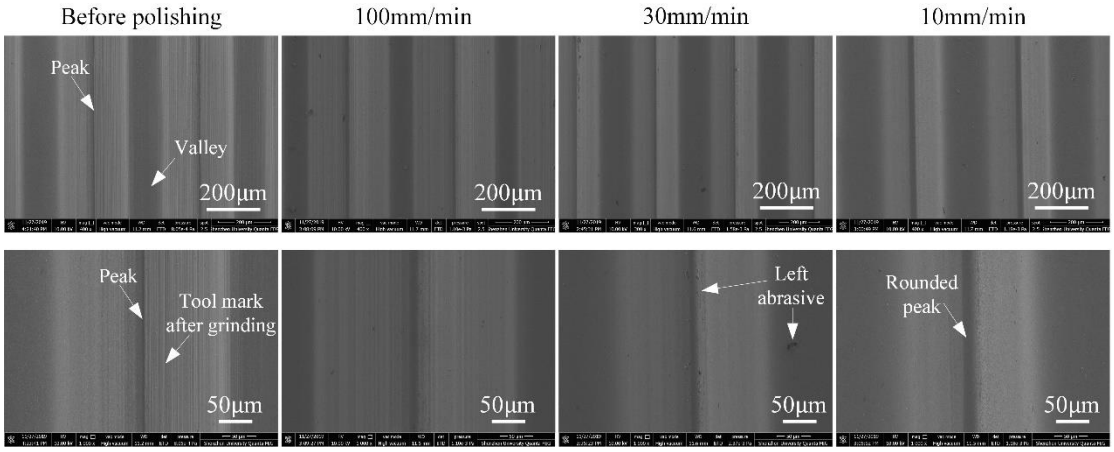

Fig. 9 Selected SEM photographs under different feed rates

The feature form profile of the V-groove was also measured to evaluate the form maintainability of MFJP as shown in Fig. 10. MFJP maintains the form well ($\eta > 88\%$) when the feed rate is higher than 30 mm/min. The form maintainability ratio η was 95.3% when the feed rate was 100 mm/min, while η was 69.7% when the feed rate was 10 mm/min. Hence, a fast feed rate with short polishing time is preferred to obtain good form maintainability in MFJP of V-groove structured surface polishing, which is

also applicable to other kinds of non-continuous structured surfaces.

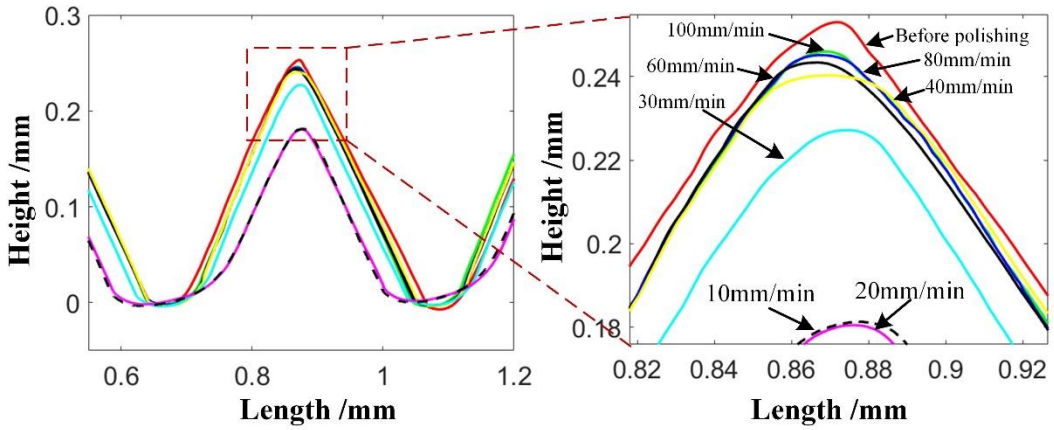

Fig. 10 Structured surface profile comparison after polishing under different feed rates

4.3 Computational fluidic dynamics (CFD) simulation

CFD simulation of FJP has been conducted previously by different researchers to demonstrate fluid field distribution and material removal characteristics during FJP. Beaucamp et al. [43] adopted the CFD model to optimize the configuration of the slurry circulation system, to obtain better polishing performance. Wang et al. [44] utilized the CFD model to develop a material removal model of FJP under both vertical and tilted impinging modes. Cheung et al. [45] used the CFD model to analyze the effect of the target surface curvature on the material removal and obtained a database of tool influence functions for various kinds of surfaces with different curvatures. Hence, the CFD method was also used in this study to investigate the flow field distribution and material removal characteristics during FJP of V-grooved surface. The CFD simulation model was built using the ANSYS FLUENT software package.

Fig. 11 shows two showcases of the developed model using FLUENT, which are the jet axis facing the peak and valley of the V-groove surface, respectively. A Eulerian-Lagrangian approach was used in this model to simulate the multiphase flow that the liquid water, air, and abrasive particles are involved in. The water and air were treated as Eulerian phases, while the abrasive particle was treated as the Lagrangian phase. Besides, the Navier–Stokes equation with incompressible form was applied to solve the fluid velocity field. Considering the effect of turbulence on the flow field, Shear-Stress Transport (SST) based on the blending of the k-ω and k-ε turbulence models was used

to express the turbulent fluid flow in the inner region of the boundary layer as well as in the outer part of the boundary layer for a wide range of the Reynolds number.

To describe the multiphase systems, a coupled algorithm and Volume of Fluid (VOF) model were employed to solve the pressure-velocity coupling and model the continuous multiphase, respectively. A random walk model and two-way coupling method were used to simulate the interaction between the discrete phase and continuum phase. Oka's erosion model was employed to determine the material erosion resulting from the abrasive impact. The fluid pressure of the inlet was 8 bar. Other detailed settings can be found in the previous publication by the authors [44].

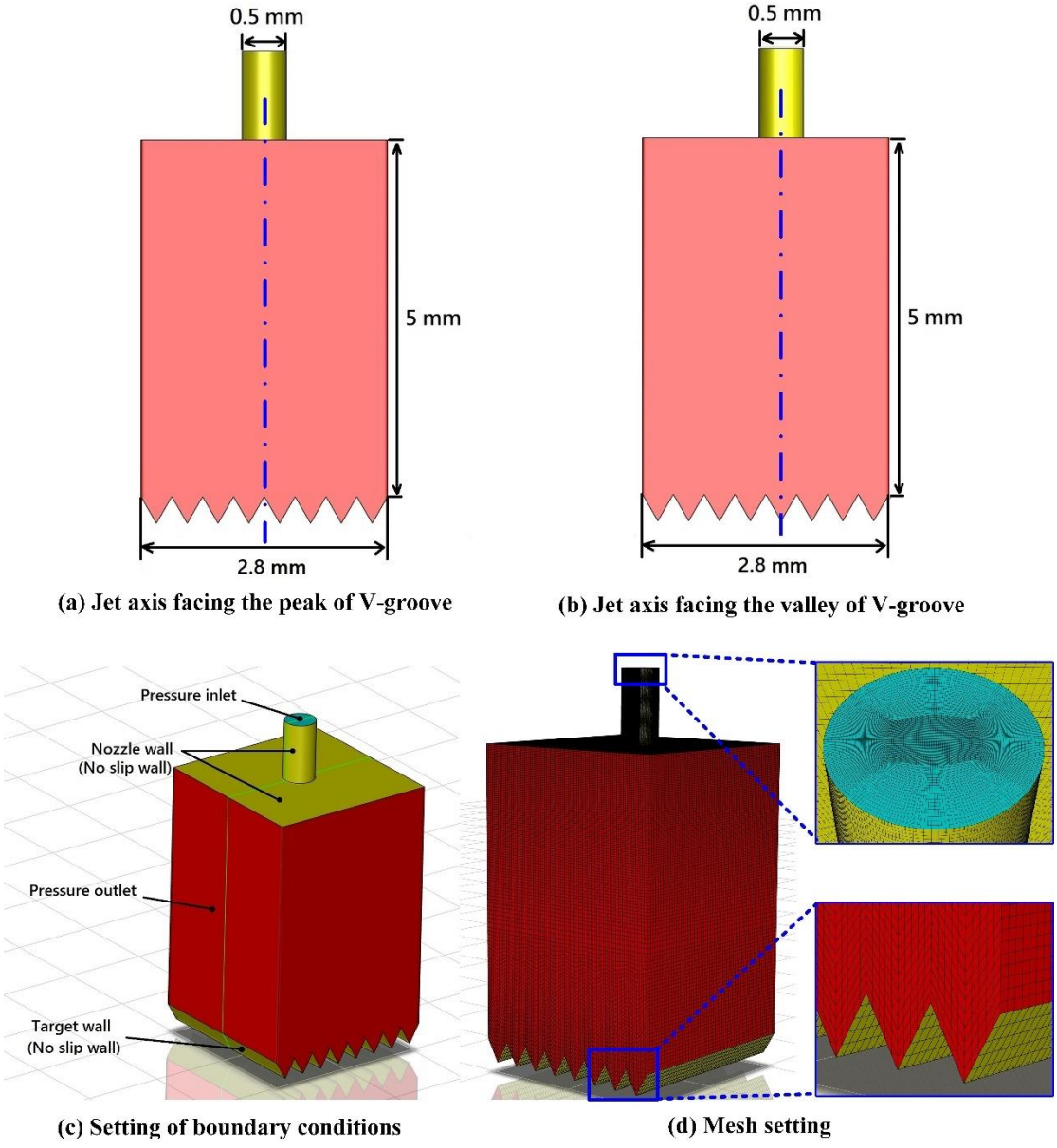

Fig. 11 Computational fluidic dynamic model of maskless fluid jet polishing V-groove

surface

The simulation result is demonstrated in Fig. 12. It is noted that the velocity distribution in MFJP for V-groove surface is quite different from the case of FJP on flat or curved surfaces as presented by Wang et al. [44]. The fluid flow is guided to concentrate along a direction parallel to the groove direction after impinging, while the fluid flow perpendicular to the groove direction is blocked as shown in the velocity distribution in Fig. 12. Hence, the material removal distribution is not rotationally symmetrically distributed. Moreover, the shape of the material removal distribution in these two cases were also different from each other, induced by the different fluid flow movement. It is also noted that the material removal on the peak surface was larger than the valley position in these two cases, which suggests that the form change of the peak is the main reason for form deviation as demonstrated in section 4.2.

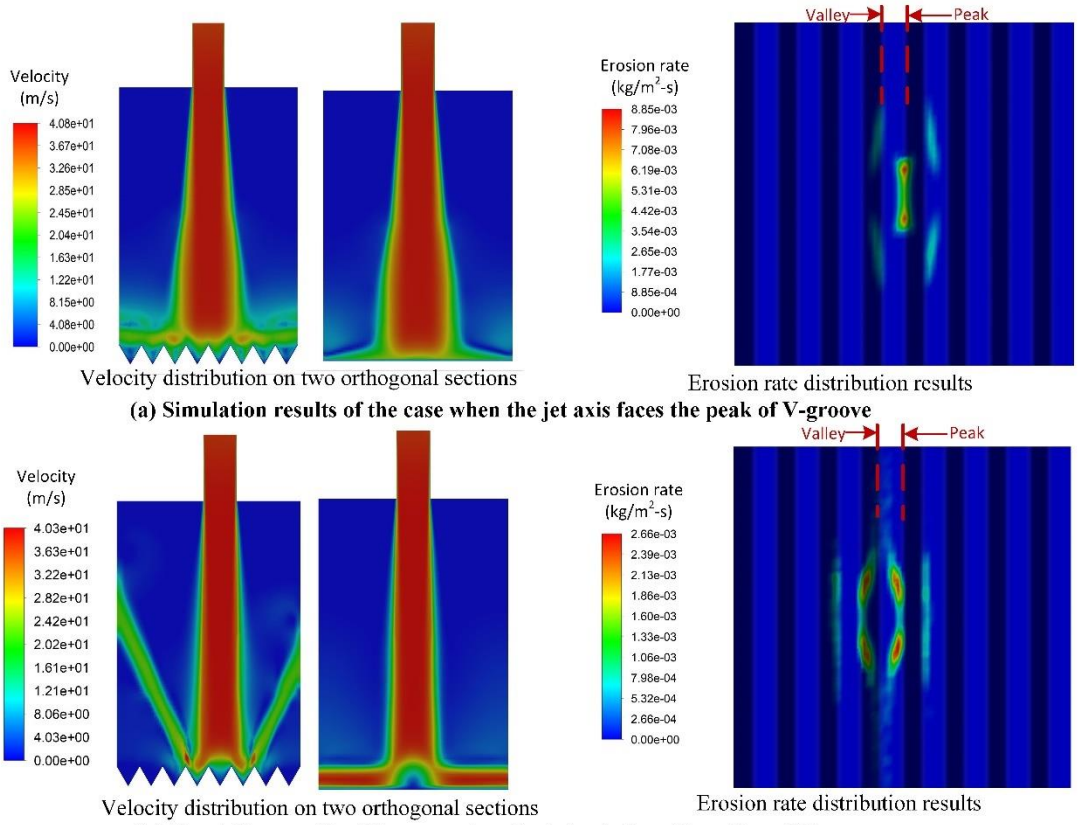

Fig. 12 Simulation results of the velocity and erosion rate distribution

4.4 Analysis of the effect of key polishing parameters

4.4.1 Effect of fluid pressure

Fluid pressure is a key parameter in FJP. It can directly determine the impinging velocity of the fluid jet, which can significantly affect the polishing performance. Fig. 13 shows the surface roughness after polishing under different pressure, and it is found that the minimum surface roughness was obtained when the fluid pressure was 8 bar. When the fluid pressure was higher than 8 bar, it resulted in higher surface roughness. This can be explained by the fact that the abrasive in the fluid jet can attain a higher impinging speed under higher fluid pressure, leading to deeper indentation of each abrasive on the target surface, which can result in larger surface roughness. According to the material removal model of FJP developed by Cao and Cheung [46], the volume of material removal by a single abrasive V can be expressed as

$$V = k\left(\frac{1}{2}m_p v_t^{\,2}\right)\left(\frac{1}{2}m_p v_n^{\,2}\right)^{\frac{2(1-b)}{3}} \tag{4}$$

where k is a material dependent coefficient, m_p is the mass of abrasive particle, v_t is the tangential velocity to the target surface, v_n is the normal velocity to the target surface, and b ($0.5 \le b \le 1$) is a material dependent exponent of the cross-section area of abrasive indentation. Higher fluid pressure can lead to a higher value of v_t and v_n, generating a larger material removal amount by a single abrasive particle, which can also be reflected from the simulated velocity and erosion rate simulation results as shown in Fig. 13.

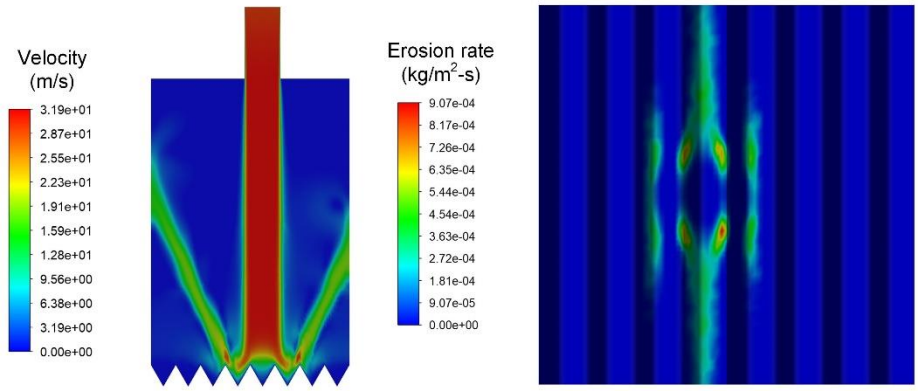

(a) Pressure = 6 bar

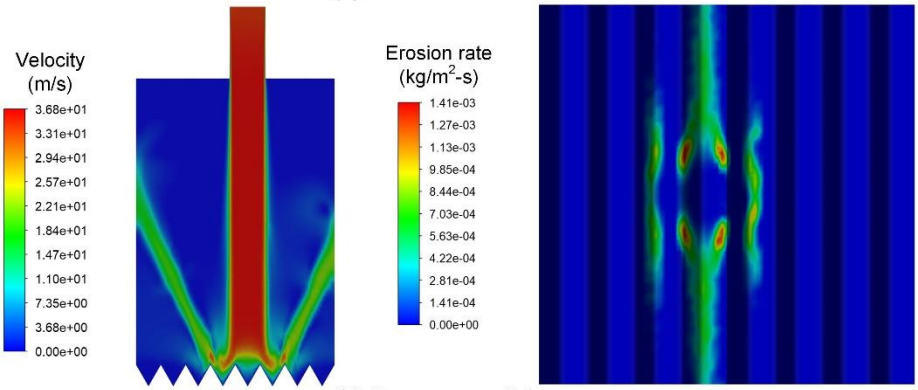

(b) Pressure = 8 bar

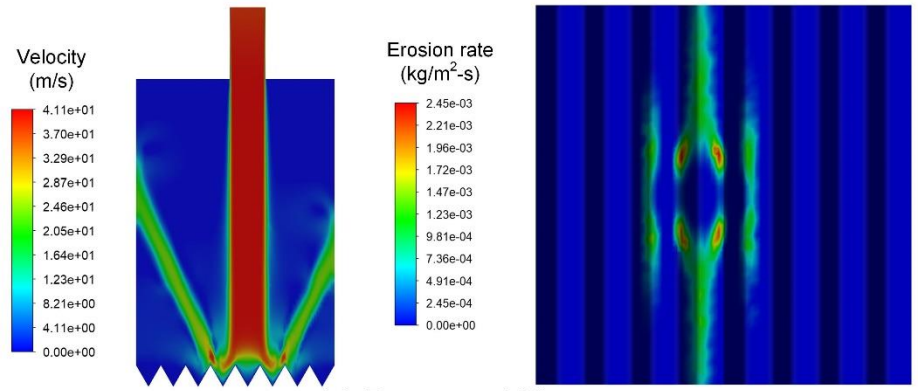

(c) Pressure = 10 bar

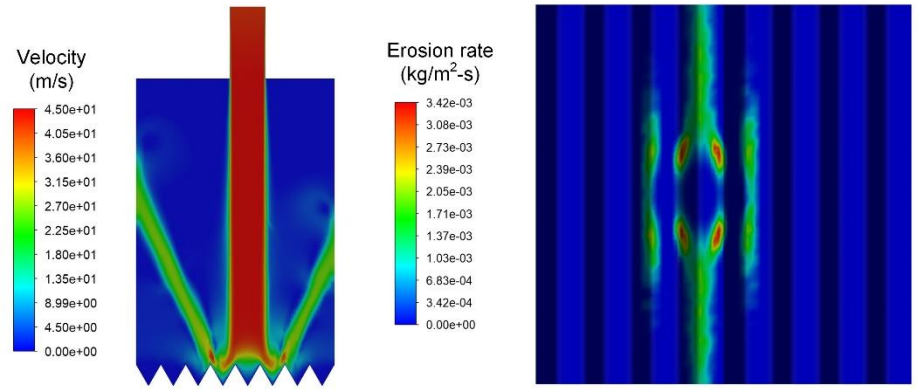

(d) Pressure = 12 bar

Fig. 13 Simulation results of velocity and erosion rate distribution in fluid jet polishing of V-groove surface under different pressure

As for the reason for higher surface roughness under 6 bar of fluid pressure, it could be attributed to the small material removal in this case, which can also be explained by Eq. (4). As shown in the SEM photographs under different fluid pressure in Fig. 15, most of the grinding tool marks still exist on the V-groove surface when the fluid pressure is 6 bar, which further confirms the insufficient material removal under low fluid pressure.

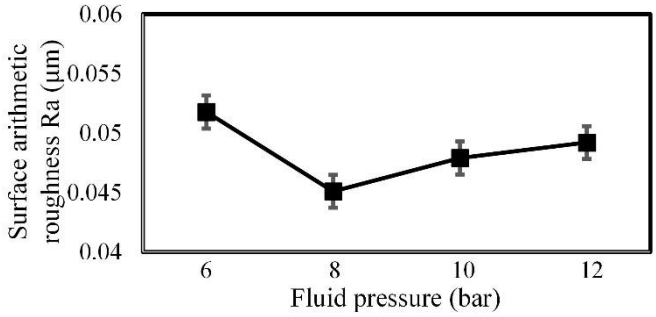

Fig. 14 Measured surface arithmetic roughness under different fluid pressure

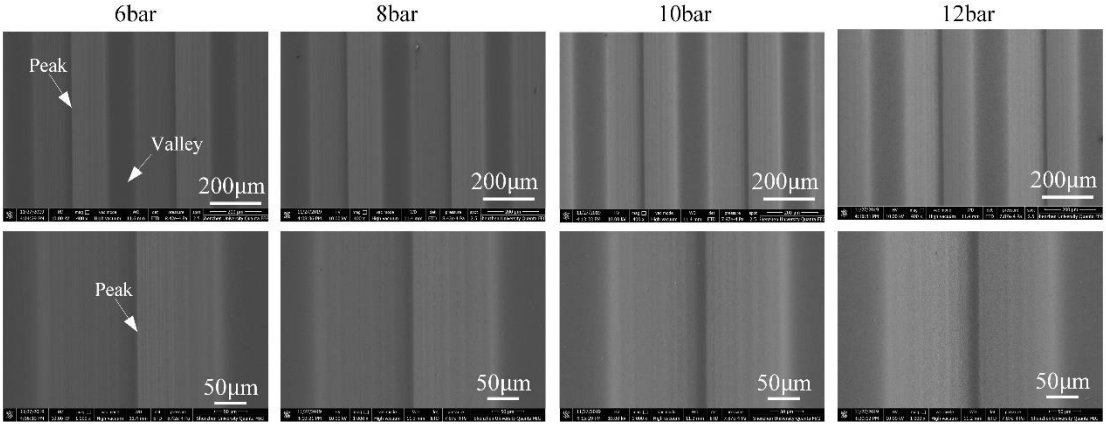

Fig. 15 SEM photographs under different fluid pressure

The form profile under different fluid pressure is also demonstrated in Fig. 16. It is interesting to note that high fluid pressure can lead to low form maintenance. The form maintenance ratio was 91.9% after polishing with 8 bar of fluid pressure, while η was 84.0% when the fluid pressure was 12 bar.

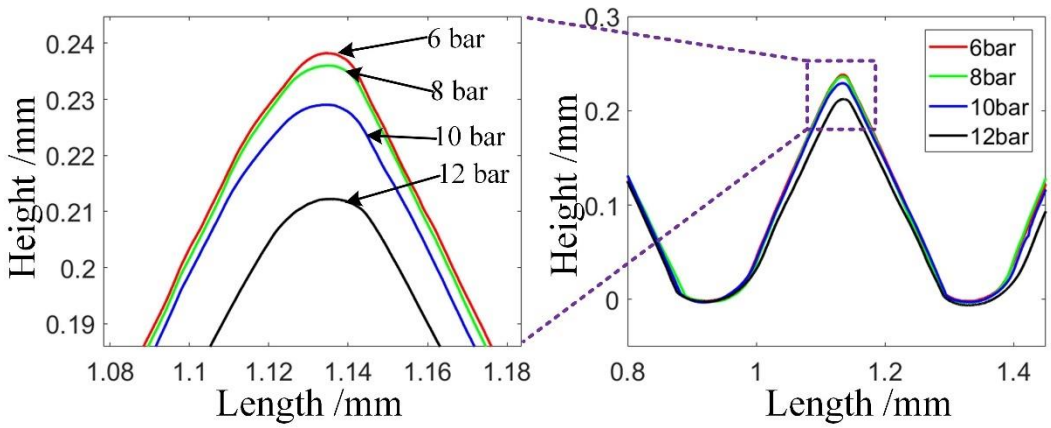

Fig. 16 Structured surface profile comparison after polishing under different fluid pressure

4.4.2 Effect of impinging angle

The impinging angle ($0^\circ < \alpha \leq 90^\circ$) is the angle between the fluid jet and the target surface plane, which determines the impinging direction of the abrasive particles. Hence, a suitable impinging angle should be considered before MFJP of structured surface. Impinging angles of 45, 60, 75 and 90 degrees were compared in this study. An impinging angle of less than 45 degrees was not considered in this study due to the interference between the nozzle and the target surface during polishing. The surface roughness of the V-groove surface after polishing under different impinging angles is demonstrated in Fig. 17. It is noted that a large impinging angle is not beneficial for obtaining low surface roughness. MFJP with an impinging angle of 45 degrees can achieve the lowest surface roughness as shown in Fig. 17, that is, 43.6 nm on average.

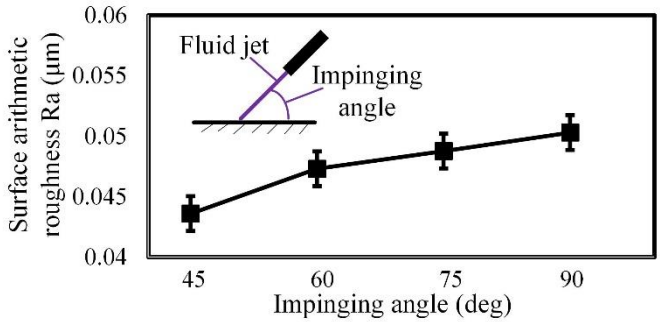

Fig. 17 Measured surface arithmetic roughness under different impinging angles

The generation of surface roughness is directly related to the material removal volume by a single abrasive particle. As described in Cao and Cheung's model [46], the volume removal by a single abrasive particle can be decomposed into the sum of normal and tangential components. The normal component of the volume removal V_N is critical in the determination of surface roughness, which can be expressed as

$$V_N = k\frac{m_p^{1+n} v_0^{2(1+n)} \sin^{2(1+n)} \alpha}{p_n} \tag{5}$$

where k and n are positive constants determined by the experiments, v_0 is the initial velocity of the particle before impinging, and p_n is the normal component of the contact pressure between the particle and target surface. Hence, it can be seen from Eq. (5) that V_N is positively related to impinging angle α, which explains the phenomenon of larger impinging angle resulting in higher surface roughness.

Fig. 18 shows SEM photographs of the V-groove surface after polishing under different impinging angles, and the form profile of them are compared in Fig. 19. It is interesting to note that a smaller impinging angle is also beneficial for form maintenance, which can also be explained by the smaller removal volume in the normal direction of a single abrasive particle as expressed in Eq. (4).

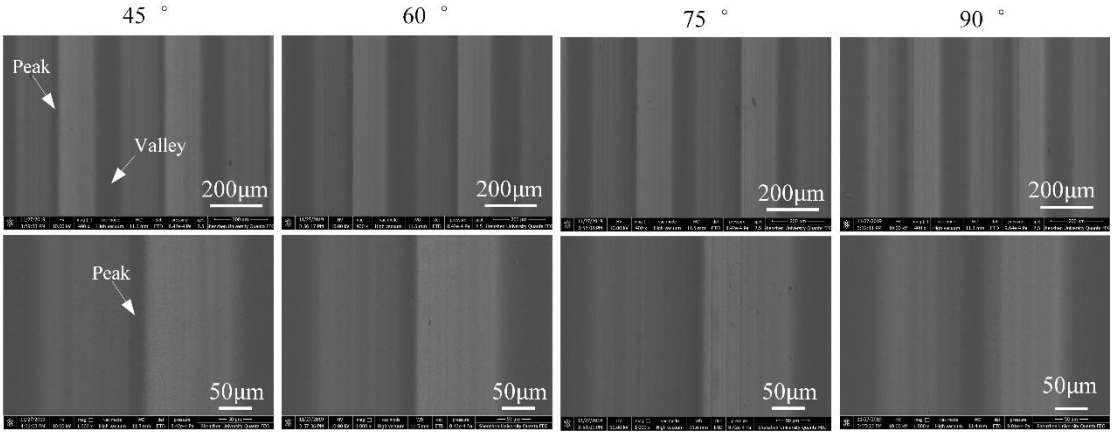

Fig. 18 SEM photographs under different impinging angles

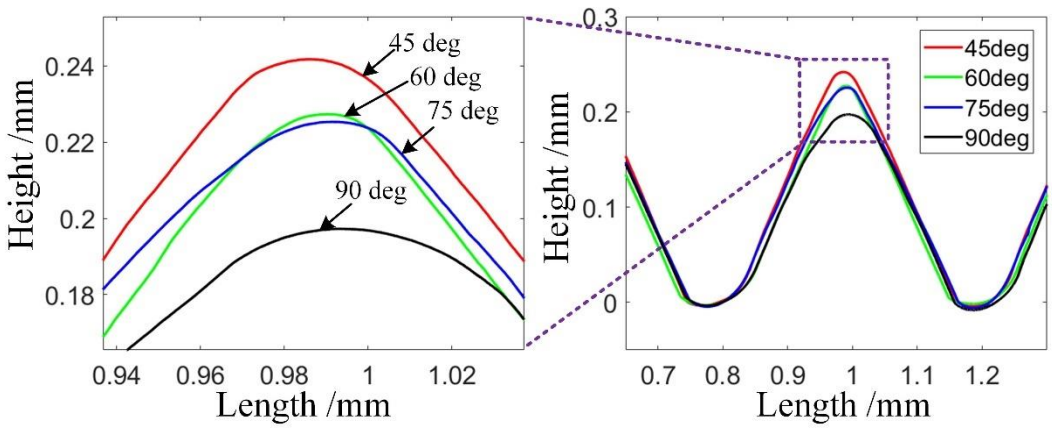

Fig. 19 Structured surface profile comparison after polishing under different impinging angles

4.4.3 Effect of stand-off distance

The stand-off distance (SOD) is not larger than 20 times the jet diameter for normal FJP. Hence, SODs of 2 mm, 4 mm, 6 mm, 8 mm, and 10 mm were investigated in this study. The surface roughness results of the V-groove surface after polishing under different SODs are demonstrated in Fig. 20. The result indicates that the effect of SOD on the final surface roughness is not obvious within the suitable range of SOD, which is consistent with the performance when polishing other kinds of surfaces as reported by Wang et al. [47]. Nevertheless, the SOD cannot be too small, because some abrasive particles in the fluid jet cannot reach the same velocity as the jet due to collisions on the way to the nozzle outlet, resulting in insufficient impact for material removal or a low material removal rate. As shown in Fig. 21, the material removal rate was the lowest when the SOD was 2 mm. When the SOD was in the range of 4 mm to 8 mm, the material removal rate of them was close to each other. Moreover, the effect of SOD on surface topography and form maintenance is also negligible, as revealed by the results of the SEM photographs and form profile comparison results in Fig. 22 and Fig. 23, respectively. The SOD can affect the impinging velocity of the abrasive in the fluid jet, but the variance of the velocity is small within the working range of SOD, leading to a tiny fluctuation of the material removal according to Eq. (4).

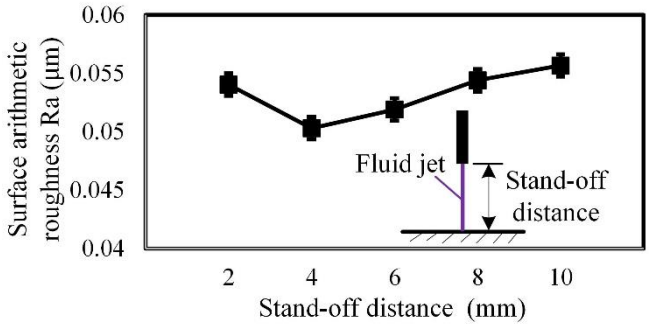

Fig. 20 Measured surface arithmetic roughness under different stand-off distances

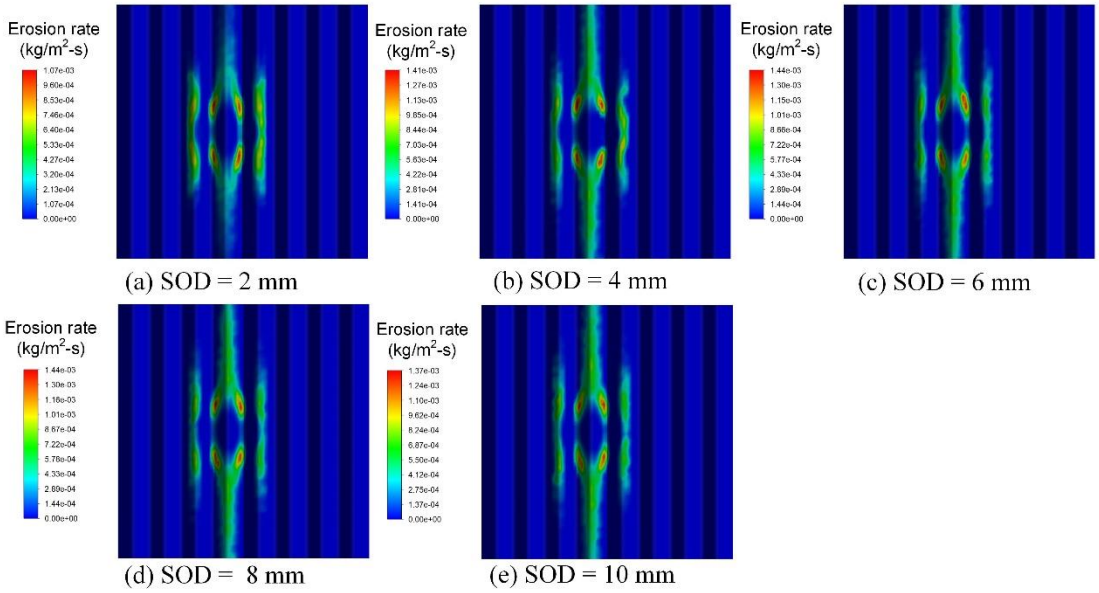

Fig. 21 Simulation results for the erosion rate distribution under different stand-off distances

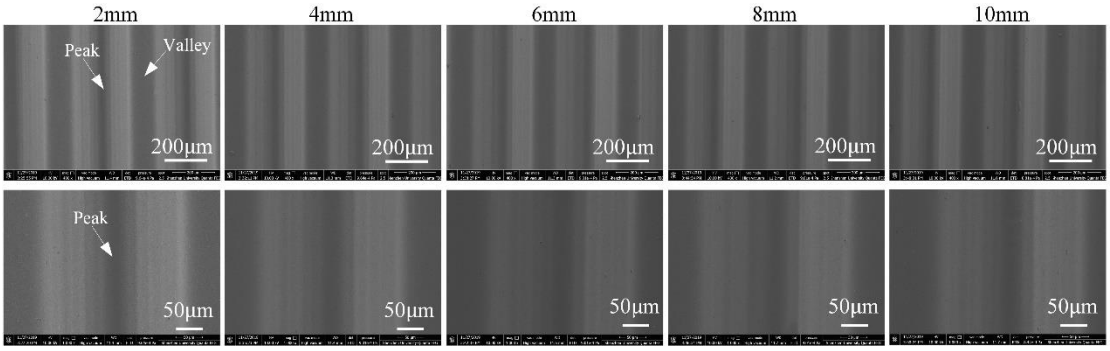

Fig. 22 SEM photographs under different stand-off distances

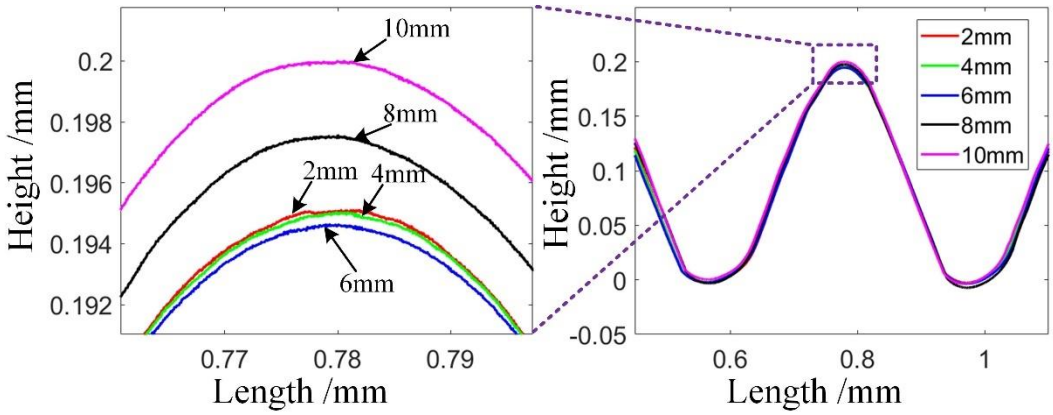

Fig. 23 Structured surface profile comparison after polishing under different stand-off distances

5. Conclusions

Maskless fluid jet polishing (MFJP) is proposed for the precision polishing of optical structured surfaces, which may provide a turnkey solution for the precision production of high-accuracy intricate optical structured surfaces. As compared to abrasive water jet machining or fluid jet polishing, no mask is needed during MFJP of structured surface due to to its low fluid pressure. A feasibility study was conducted on both continuous (i.e., sinusoidal structured surface) and dis-continuous structured surface (i.e., V-groove structured surface), as well as a systematic study of the effect of key parameters. The main findings can be summarized as follows:

(a) Surface defects on sinusoidal structure surface generated by wire EDM machining are considerably diminished by FJP, obtaining a highly smooth surface. The surface roughness on the top and bottom position was reduced from 642.1 nm and 458.9 nm to 18.8 nm and 14.4 nm, respectively. Meanwhile, the surface form maintenance ratio reached 99.8%, which indicates high form maintainability. It demonstrates the superior polishing performance of MFJP on sinusoidal structured surface. Moreover, it also sheds some light on the good polishing performance on other continuous structured surfaces.

(b) The grinding marks on V-groove structured surface can be completely removed by MFJP. The average surface roughness can be reduced from 132.5 nm to 40.6 nm

after one pass of polishing, while obtaining a form maintenance ratio of more than 95% under certain conditions. This proves that MFJP is also suitable for the polishing of V-groove structured surface under proper polishing conditions.

(c) High fluid pressure is unfavorable for obtaining good form maintainability. Moreover, a small impinging angle is beneficial for obtaining good surface roughness. The effect of the stand-off distance is not obvious, which is the same as for FJP in other applications.

MFJP is effective for the polishing of optical structured surfaces in applications without stringent requirements regarding structure form accuracy, such as illumination field. This study also sheds some light on the application of MFJP for the post processing of other components which have small or micrometer-scale cavities or channels, such as microfluidic channels, etc. Moreover, nanometer-scale polishing abrasives or even colloidal polishing abrasives can be used for surfaces with stringent surface roughness requirements.

However, it should be noted that the form maintainability of MFJP on discontinuous structured surface is not high under a long polishing time. Hence, the surface roughness of discontinuous structured surface should be good enough to reduce the polishing time in MFJP to implement high form maintainability. Moreover, the polishing efficiency of MFJP is lower than that of the mechanical polishing method, leading to a long polishing time when polishing large surfaces, which should be further improved in the future.

CRediT authorship contribution statement

Chunjin Wang: Conceptualization, Methodology, Investigation, Formal analysis, Writing-original draft, Funding acquisition. **Zili Zhang:** Methodology and Formal analysis. **Chi Fai Cheung:** Conceptualization, Funding acquisition, Resources, Writing-review and editing. **Wang Luo:** Formal analysis. **Yee Man Loh:** Investigation**.** **Yanjun Lu:** Conceptualization, Methodology, Formal analysis, Writing-review and

editing. **Lingbao Kong:** Conceptualization, Writing-review and editing. **Shixiang Wang**: Formal analysis.

Declaration of Competing Interest

The authors report no declarations of interest.

Acknowledgement

The work described in this paper was mainly supported by a grant from the Research Grants Council of the Government of the Hong Kong Special Administrative Region, China (Project No. 15200119) and the financial support from the Guangdong Natural Science Foundation Program 2019-2020 (Project No.: 2019A1515012015). In addition, the authors would also like to express their sincere thanks to the funding support from International Partnership Scheme of the Bureau of the International Scientific Cooperation of the Chinese Academy of Sciences (Project No.: 181722KYSB20180015) and the Research Office of The Hong Kong Polytechnic University for the research studentships (Project codes: RK3M).

References

[1] Evans C. J., and Bryan J. B., 1999. “Structured”, “Textured” or “Engineered” Surfaces. CIRP Annals - Manufacturing Technology, 48(2), 541-556.

[2] Zhang, S., Zhou, Y., Zhang, H., Xiong, Z., and To, S., 2019. Advances in ultra-precision machining of micro-structured functional surfaces and their typical applications. International Journal of Machine Tools and Manufacture, 142, 16-41.

[3] Yan, G., Zhang, Y., You, K., Li, Z., Yuan, Y., and Fang, F., 2019. Off-spindle-axis spiral grinding of aspheric microlens array mold inserts. Optics express, 27(8), 10873-10889.

[4] Zhu, W. L., Duan, F., Zhang, X., Zhu, Z., and Ju, B. F., 2018. A new diamond machining approach for extendable fabrication of micro-freeform lens array. International Journal of Machine Tools and Manufacture, 124, 134-148.

[5] Jiang, D., Fan, P., Gong, D., Long, J., Zhang, H., and Zhong, M., 2016. High-temperature imprinting and superhydrophobicity of micro/nano surface structures on metals using molds fabricated by ultrafast laser ablation. Journal of Materials Processing Technology, 236, 56-63.

[6] Sun, Z., To, S., Wang, S., and Du, J., 2020. Development of self-tuned diamond milling system for fabricating infrared micro-optics arrays with enhanced surface uniformity and machining efficiency. Optics Express, 28(2), 2221-2237.

[7] Zhu, Z., To, S., and Zhang, S., 2015. Theoretical and experimental investigation on the novel end-fly-cutting-servo diamond machining of hierarchical micro-nanostructures. International journal of machine tools and manufacture, 94, 15-25.

[8] Guo, B. and Zhao, Q., 2017. Ultrasonic vibration assisted grinding of hard and brittle linear micro-structured surfaces. Precision Engineering, 48, 98-106.

[9] Brinksmeier, E., and Schönemann, L., 2014. Generation of discontinuous microstructures by diamond micro chiseling. CIRP Annals, 63(1), 49-52.

[10] He, Z. R., Luo, S. T., Liu, C. S., Jie, X. H., and Lian, W. Q., 2019. Hierarchical micro/nano structure surface fabricated by electrical discharge machining for anti-fouling application. Journal of Materials Research and Technology, 8(5), 3878-3890.

[11] Temmler, A., Liu, D. M., Drinck, S., Luo, J. B., and Poprawe, R., 2020. Experimental investigation on a new hybrid laser process for surface structuring by vapor pressure on Ti6Al4V. Journal of Materials Processing Technology, 277, 116450.

[12] Park, D. S., Cho, M. W., Lee, H., and Cho, W. S., 2004. Micro-grooving of glass using micro-abrasive jet machining. Journal of materials processing technology, 146, 234-240.

[13] Brinksmeier, E., Riemer, O., Gessenharter, A., and Autschbach, L., 2004. Polishing of structured molds. CIRP Annals, 53(1), 247-250.

[14] Brinksmeier, E., Riemer, O., and Gessenharter, A., 2006. Finishing of structured surfaces by abrasive polishing. Precision Engineering, 30(3), 325-336.

[15] Riemer, O., 2008. A review on machining of micro-structured optical molds. Key Engineering Materials 364, 13-18.

[16] Klocke F, Brinksmeier E, Riemer O, Klink, A., Schulte, H., and Sarikaya, H., 2007. Manufacturing structured tool inserts for precision glass moulding with a combination of diamond grinding and abrasive polishing. Industrial Diamond Review, 67,65-69.

[17] Zhao, Q., Sun, Z., and Guo, B., 2016. Material removal mechanism in ultrasonic vibration assisted polishing of micro cylindrical surface on SiC. International Journal of Machine Tools and Manufacture, 103, 28-39.

[18] Suzuki, H., Okada, M., Yamagata, Y., Morita, S., and Higuchi, T., 2012. Precision grinding of structured ceramic molds by diamond wheel trued with alloy metal. CIRP annals, 61(1), 283-286.

[19] Kawakubo H., and Yomogida T., 2006. Finishing Characteristics of R-Groove using Magnetic Field Assisted Machining Method. Proceedings of JSPE Semestrial Meeting. The Japan Society for Precision Engineering, 733-734.

[20] Takebayashi, Y., Hirogaki, T., Aoyama, E., Ogawa, K., and Melkote, S. N., 2013, November. Development of Magnetic Polishing for Micro Channel with a Ball-Nose-Shaped Tool. In ASME 2013 International Mechanical Engineering Congress and Exposition. American Society of Mechanical Engineers Digital Collection.

[21] Guo, J., Liu, K., Wang, Z., and Tnay, G. L., 2017. Magnetic field-assisted finishing of a mold insert with curved microstructures for injection molding of microfluidic chips. Tribology International, 114, 306-314.

[22] Kim W. B., Lee, S. H., and Min, B. K., 2004. Surface Finishing and Evaluation of Three-Dimensional Silicon Microchannel Using Magnetorheological Fluid. Journal of Manufacturing Science & Engineering, 126, 772-778.

[23] Yamaguchi, H., Riveros, R. E., Mitsuishi, I., Takagi, U., Ezoe, Y., Yamasaki, N., Mitsuda, K., and Hashimoto, F., 2010. Magnetic field-assisted finishing for micropore X-ray focusing mirrors fabricated by deep reactive ion etching. CIRP annals, 59(1), 351-354.

[24] Riveros, R.E., Yamaguchi, H., Boggs, T., Mitsuishi, I., Mitsuda, K., Takagi, U., Ezoe, Y., Ishizu, K., and Moriyama, T., 2012. Magnetic Field-Assisted Finishing of Silicon Microelectromechanical Systems Micropore X-Ray Optics. Journal of manufacturing science and engineering, 134(5).

[25] Suzuki, H., Okada, M., Lin, W., Morita, S., Yamagata, Y., Hanada, H., Araki, H., and Kashima, S., 2014. Fine finishing of ground DOE lens of synthetic silica by magnetic field-assisted polishing. CIRP Annals. 63, 313-6.

[26] Shimada, K., Wu, Y., and Wong, Y. C., 2003. Effect of magnetic cluster and magnetic field on polishing using magnetic compound fluid (MCF). Journal of magnetism and magnetic materials, 262(2), 242-247.

[27] Guo, H., Wu, Y., Lu, D., Fujimoto, M., and Nomura, M., 2014. Effects of pressure and shear stress on material removal rate in ultra-fine polishing of optical glass with magnetic compound fluid slurry. Journal of Materials Processing Technology, 214, 2759-2769.

[28] Wang Y., Wu Y., and Nomura M., 2016. Feasibility study on surface finishing of miniature V-grooves with magnetic compound fluid slurry. Precision Engineering, 45:67-78.

[29] Zhang, C., Rentsch, R., and Brinksmeier, E., 2005. Advances in micro ultrasonic assisted lapping of microstructures in hard–brittle materials: a brief review and outlook. International Journal of Machine Tools and Manufacture, 45(7-8), 881-890.

[30] Suzuki, H., Hamada, S., Okino, T., Kondo, M., Yamagata, Y., and Higuchi, T., 2010. Ultraprecision finishing of micro-aspheric surface by ultrasonic two-axis vibration assisted polishing. CIRP annals. 59(1):347-50.

[31] Guo, J., Morita, S. Y., Hara, M., Yamagata, Y., and Higuchi, T., 2012. Ultra-precision finishing of micro-aspheric mold using a magnetostrictive vibrating polisher. CIRP annals. 61, 371-4.

[32] Wang, G., Lv, B., Zheng, Q., Zhou, H., and Liu, Z., 2019. Polishing trajectory planning of three-dimensional vibration assisted finishing the structured surface. AIP Advances, 9(1), 015012.

[33] Guo, J., Jong, H. J. H., Kang, R., and Guo, D., 2018. Novel localized vibration-assisted magnetic abrasive polishing method using loose abrasives for V-groove and Fresnel optics finishing. Optics express, 26, 11608-11619.

[34] Guo, J., Feng, W., Jong, H. J. H., Suzuki, H., and Kang, R., 2020. Finishing of rectangular microfeatures by localized vibration-assisted magnetic abrasive polishing method. Journal of Manufacturing Processes, 49, 204-213.

[35] Matsumura, T., Muramatsu, T., and Fueki, S., 2011. Abrasive water jet machining of glass with stagnation effect. CIRP annals, 60, 355-358.

[36] Fähnle, O. W., Van Brug, H., and Frankena, H. J., 1998. Fluid jet polishing of optical surfaces. Applied optics, 37, 6771-6773.

[37] Lu, Y., Luo, W., Wu, X., Xu, B., Wang, C., Li, J., and Li, L., 2020. Fabrication of Micro-Structured LED Diffusion Plate Using Efficient Micro Injection Molding and Micro-Ground Mold Core. Polymers, 12(6), 1307.

[38] Bisaria, H., and Shandilya, P., 2019. Experimental investigation on wire electric discharge machining (WEDM) of Nimonic C-263 superalloy. Materials and Manufacturing Processes, 34(1), 83-92.

[39] Wang, C. J., Cheung, C. F., Ho, L. T., Liu, M. Y., and Lee, W. B., 2017. A novel multi-jet polishing process and tool for high-efficiency polishing. International Journal of Machine Tools and Manufacture, 115, 60-73.

[40] Wang, C. J., Cheung, C.F., Ho, L.T., and Loh, Y.M., 2021. Development of a fluid line-jet polishing process for rotational axisymmetric surfaces. Journal of Manufacturing Processes, 61, 15-24.

[41] Liu, M. Y., Cheung, C. F., Feng, X., Wang, C. J., and Cao, Z. C., 2020. Any-degrees-of-freedom (anyDOF) registration for the characterization of freeform surfaces. Precision Engineering, 62, 170-180.

[42] Whitehouse DJ. Surfaces and their Measurement. CRC Press; 2002.

[43] Beaucamp, A., Namba, Y., and Freeman, R., 2012. Dynamic multiphase modeling and optimization of fluid jet polishing process. CIRP annals, 61(1), 315-318.

[44] Wang, C. J., Cheung, C.F., and Liu, M. Y., 2017. Numerical modeling and experimentation of three dimensional material removal characteristics in fluid jet polishing. International Journal of Mechanical Sciences, 133, 568-577.

[45] Cheung, C. F., Wang, C. J., Ho, L. T., and Chen, J., 2018. Curvature-adaptive multi-jet polishing of freeform surfaces. CIRP Annals, 67(1), 357-360.

[46] Cao, Z. C., and Cheung, C. F., 2014. Theoretical modelling and analysis of the material removal characteristics in fluid jet polishing. International Journal of Mechanical Sciences, 89, 158-166.

[47] Wang, C. J., Cheung, C. F., Ho, L. T., and Loh, Y. M., 2020. An Investigation of Effect of Stand-Off Distance on the Material Removal Characteristics and Surface Generation in Fluid Jet Polishing. Nanomanufacturing and Metrology, 1-11.